First-principles Investigation of Aluminum Intercalation and Diffusion in TiO_2 Materials: Anatase versus Rutile

Weiqiang Tang[1], Jin Xuan[2], Huizhi Wang[3,*], Shuangliang Zhao[1,*], Honglai Liu[4]

[1] School of Chemical Engineering and State Key Laboratory of Chemical Engineering, East China University of Science and Technology, Shanghai, 200237, China

[2] School of Engineering and Physical Sciences, Heriot-Watt University, Edinburgh, EH14 4AS, United Kingdom

[3] Department of Mechanical Engineering, Imperial College London, Exhibition Road, South Kensington Campus, London, SW7 2AZ, United Kingdom

[4] School of Chemistry and Molecular Engineering, East China University of Science and Technology, Shanghai, 200237, China

* Correspondence and requests for materials should be addressed to H.W. (email: huizhi.wang@imperial.ac.uk) or to S.Z. (email: szhao@ecust.edu.cn).

Abstract

Aluminum-ion batteries, emerging as a promising post-lithium battery solution, have been a subject of increasing research interest. Yet, most existing aluminum-ion research has focused on electrode materials development and synthesis. There has been a lack of fundamental understanding of the electrode processes and thus theoretical guidelines for electrode materials selection and design. In this study, by using density functional theory, we for the first time report a first-principles investigation on the thermodynamic and kinetic properties of aluminum intercalation into two common TiO_2 polymorphs, i.e., anatase and rutile. After examining the aluminum intercalation sites, intercalation voltages, storage capacities and aluminum diffusion paths in both cases, we demonstrate that the stable aluminum intercalation site locates at the center of the O_6 octahedral for TiO_2 rutile and off center for TiO_2 anatase. The maximum achievable Al/Ti ratios for rutile and anatase are 0.34 and 0.36p, respectively. Although rutile is found to have an aluminum storage capacity slightly higher than anatase, the theoretical specific energy of rutile can reach 20.90 Wh kg^{-1}, nearly twice as high as anatase (9.84 Wh kg^{-1}). Moreover, the diffusion coefficient of aluminum ions in rutile is 10^{-9} cm^2 s^{-1}, significantly higher than that in anatase (10^{-20} cm^2 s^{-1}). In this regard, TiO_2 rutile appears to be a better candidate than anatase as an electrode material for aluminum-ion batteries.

Keywords: Aluminum-ion batteries; Titanium dioxide electrode; First-principles calculations; Intercalation mechanisms; Mesoscale

Nomenclature

a, b, c	Lattice parameters (Å)
d	Hopping distance of ions (Å)
D	Diffusion coefficient ($cm^2\ s^{-1}$)
E	Internal (potential) energy ($kJ\ mol^{-1}$)
ΔE_a	Activation energy ($kJ\ mol^{-1}$)
F	Faraday's constant, 96485 A s mol^{-1}
g	Geometric factor
G	Gibbs free energy ($kJ\ mol^{-1}$)
k_B	Boltzmann constant, 1.38×10^{-23} J K^{-1}
M_V	Molar volume ($L\ mol^{-1}$)
M_W	Molar weight ($g\ mol^{-1}$)
T	Temperature (K)
v	Atomic vibration frequency (s^{-1})
$V(x)$	Average voltage (V)
x	Molar fraction
x_{max}	Theoretical maximum concentration
z	Number of electrons involved in electrode

Greek symbols

α, β, γ	Lattice parameters (deg)
ε_M	Gravimetric energy density ($Wh\ kg^{-1}$)
ε_V	Volumetric energy density ($Wh\ L^{-1}$)

1. Introduction

The rapidly increasing penetration of renewable energies has urged the development of efficient battery storage techniques. Although lithium ion batteries (LIBs), currently enjoying a great market success in consumer electronics, have attracted the most attention as a candidate for transport and grid applications [1-4], the high cost, lithium availability and safety concerns associated with LIBs necessitate the development of alternative battery solutions. Aluminum-ion batteries that rely on the principle of reversible intercalation of chloroaluminate ($[Al_xCl_y]^-$) or aluminum ions have emerged as a promising post-lithium solution since 2010 when they were invented [5]. The use of aluminum instead of lithium in rocking chair batteries offers many advantages, including (i) potentially low cost due to the abundance of aluminum resources, (ii) improved safety by eliminating the need for flammable organic electrolytes, and (iii) high theoretical capacity due to the trivalent nature of aluminum ions.

Identifying suitable electrode materials with high energy and power capabilities lies at the heart of the R&D of aluminum ion batteries. In contrast to monovalent lithium ions, the high valence state of aluminum ions together with their small ionic radii (54 pm for Al^{3+} versus 76 pm for Li^+) make their intercalation into a host crystal structure challenging [6-8]. Among different potential electrode materials, TiO_2, a widely studied material for electrochemical lithium storage, is of particular interest due to its attractive features such as good structural stability, low toxicity, high safety and low cost. It has been reported that eight types of crystal structures exist for TiO_2 material [9]. In 2012, Liu et al. [10] demonstrated for the first time the reversible intercalation of Al^{3+} ions into TiO_2 with anatase TiO_2 nanotube arrays in an aqueous $AlCl_3$ electrolyte. They confirmed that the redox of Ti^{4+}/Ti^{3+} was responsible for the reversible storage of Al^{3+} ions in TiO_2. A specific capacity of 75 mAh g^{-1} at a current density of 4 mA g^{-1} was reported in their study. The Al^{3+} storage performance was shown to be significantly improved by employing black anatase TiO_2 nanoleaves [11] and high-surface-area anatase

TiO_2 nanospheres [12], which respectively achieved 278 mAh g^{-1} (at 50 mA g^{-1}) and 183 mAh g^{-1} (at 50 mA g^{-1}). Very recently, we demonstrated good aluminum storage performance with nanosized rutile TiO_2 [13]. It is noted that aluminum intercalation in TiO_2 has been evidenced only in aqueous electrolytes. So far, no evidence of aluminum intercalation has been reported for non-aqueous electrolytes. Despite these encouraging achievements, there is still a lack of atomic-level understanding of aluminum intercalation processes in TiO_2 materials. In particular, the thermodynamic limit and atomistic mechanisms of Al^{3+} diffusion in TiO_2 are generally unclear.

This study therefore presents a density-functional-theory (DFT) study of aluminum intercalation into two common TiO_2 polymorphs, i.e., anatase and rutile, with the aim of providing atomic-level insights into the electrode processes. The thermodynamic and kinetic behaviors associated with the two different TiO_2 polymorphs are thoroughly studied and carefully compared, which can lead to a better understanding of the battery performance and guide on further materials design for aluminum ion batteries.

2. Modelling and computational methods

All calculations were carried out by using periodic DFT within the Vienna ab initio simulation package (VASP) [14,15]. VASP provides an iterative solution of the Kohn-Sham equations of DFT upon a plane wave basis, wherein the inner cores and electron-ion interactions are described with pseudopotentials through the projected augmented wave (PAW) method [16,17]. A plane-wave basis set with a cutoff energy of 500 eV was used to expand the eigenstates of the electron wave functions. The calculation systems were established with periodic boundary conditions. A supercell containing 96 atoms with 2×2×4 unit cells was modelled for TiO_2 rutile whereas a supercell containing 108 atoms with 3×3×1 unit cells was modelled for TiO_2 anatase [18,19]. To maximize computational efficiency while not affecting the calculation accuracy, a

minimal Monkhorst-Pack 5×5×2 k-point grid was used to sample the Brillouin zones for our structure calculations. The convergence criterion for the electronic self-consistent cycle was fixed at 0.01 meV per cell. Full relaxation of all atomic positions was performed until the forces on all atoms were less than 0.1 meV $Å^{-1}$ per cell for assuring geometrical and energetic convergence. The climbing-image nudged elastic band (CI-NEB) method [20] was used to calculate the minimum energy pathways (MEPs) and the energy barriers for aluminum diffusion in the TiO_2 materials.

2.1. Aluminum intercalation voltage

It has been proposed in the previous research [10] that the electrochemical aluminum intercalation into TiO_2 follows the below reaction:

$$TiO_2 + x\ \mathrm{Al\ (metal)} \leftrightarrow \mathrm{Al}_x TiO_2, \quad (1)$$

where x is the molar fraction of aluminum. The average voltage of (1) for a composition range between 0 and x, $V(x)$ (V), can be therefore expressed as [21],

$$V(x) = -\Delta G/xzF, \quad (2)$$

where ΔG (kJ mol^{-1}) is the Gibbs free energy change due to the aluminum intercalation, F (=96485 A s mol^{-1}) is the Faraday constant, and z is the number of the charge transferred during the reaction per mole reactant (z = 3). Under ambient conditions, ΔG can be approximated with the internal (potential) energy change (ΔE) by neglecting the contribution from the configurational and vibrational entropy change due to the intercalation. While the entropy contribution can be calculated through the vibrational frequencies [22], it has been reported that this contribution is overall small compared to the internal energy at room temperatures (typical working conditions of aqueous aluminum-ion batteries), and thus can be ignored [21,23]. The change of internal energy is given by

$$\Delta E = E\left(\mathrm{Al}_x TiO_2\right) - E\left(TiO_2\right) - xE\left(\mathrm{Al}\right), \quad (3)$$

where $E(\mathrm{TiO_2})$ and $E(\mathrm{Al}_x\mathrm{TiO_2})$ are the internal energies before and after the aluminum intercalation, respectively. $E(\mathrm{Al})$ is the internal energy of aluminum metal. Since small variations in composition are required in order to calculate ΔE accurately, large supercells as described above were used in our calculation for calculating $E(\mathrm{Al}_x\mathrm{TiO_2})$ and $E(\mathrm{TiO_2})$, while *E*(Al) was obtained by optimization of face-centered cubic (*Fm3m*) Al metal with $a_0 = 4.0495$ Å [24], using a k-point mesh of 25×25×25.

2.2. Theoretical capacity and energy density

The theoretical capacity of TiO_2 can be calculated from the equation below.

$$\text{Capacity} = x_{\max} zF/3.6M_w \ (\text{mAh g}^{-1}), \quad (4)$$

where M_w (=79.866 g mol^{-1}) is the molar weight of TiO_2, and $x_{\max}$ is the theoretical maximum concentration of aluminum that the different TiO_2 structures can accommodate. $x_{\max}$ in this study is determined by the DFT calculation.

In addition to theoretical capacity, energy density is also a performance metric of interest, and it can be calculated from the thermodynamic data before and after the chemical reaction in equation (1). Energy density can be characterized by the gravimetric energy density ε_M (Wh kg^{-1}) or by the volumetric energy density ε_V (Wh L^{-1}). The gravimetric energy density of the electrode material is defined as

$$\varepsilon_M = \Delta G/M_w . \quad (5)$$

The volumetric energy density of the electrode material is defined as

$$\varepsilon_V = \Delta G/M_V . \quad (6)$$

Here M_V represents the molar volume of TiO_2, which can be calculated from the density of rutile (3.89 g cm^{-3}) and anatase (4.25 g cm^{-3}) [25-27].

From eqs. (4) to (6), the theoretical capacity and energy density can be calculated with the Gibbs formation energies determined through first principles calculations [28].

3. Results and discussion

3.1. Crystal structure and aluminum intercalation sites

As the aluminum storage properties are sensitive to the structural properties (especially to the unit cell volume) of the host lattice, it is essential to achieve an accurate prediction for the lattice parameters. For transition metal oxides, DFT+U method [29] was previously adopted to evaluate the on-site Coulomb interactions and exchange interactions in the localized *d* orbital [30,31]. The Dudarev approach is implemented in VASP in which only the difference between the Coulomb parameter U and exchange parameter J is meaningful [32].

In the DFT-GGA method, the on-site U parameter is not included, and it presents a small systematic overestimation of cell volumes. The results in Table 1 show the deviations between the calculated cell volumes with GGA method and the measured ones for both rutile and anatase. The experimental measurements were obtained by using programmed electronic X-ray automatic diffractometer (PEXRAD) [33,34]. It can be seen that the deviation is about 3.3% for rutile and 3.7% for anatase. In parallel, we also include a comparison of experimental and calculated unit cell volumes for rutile and anatase using both DFT and DFT+U (U=4.2 eV, J=0.0 eV) approaches, as shown in Table 1. The deviation of the theoretical volumes with the experimental ones increases up to 7.5% for rutile and 8.2% for anatase using DFT+U approach.

Table 1. Experimental and calculated lattice parameters for rutile and anatase TiO_2. In all cases, $\alpha=\beta=\gamma= 90^{\circ}$.

Parameter	Rutile			Anatase		
	Experiment [33]	PBE	PBE+U	Experiment [34]	PBE	PBE+U
a=b (Å)	4.594	4.661	4.694	3.784	3.826	3.902
c (Å)	2.959	2.971	3.048	9.515	9.653	9.686

Volume ($Å^3$)	62.45	64.54	67.16	136.24	141.30	147.47
ΔV (%)	/	3.3	7.5	/	3.7	8.2

These results are interesting, since the DFT calculations with pure GGA (PBE) provide a better agreement with the experimental lattice parameters, compared with the DFT+U calculation, although the latter method involves semi-empirical parameter [31]. In short, our calculations on rutile and anatase based on GGA-PBE show good consistence with the experimental results for the unit cell volume, and therefore the GGA-PBE approach is applied below for calculating the favorable aluminum intercalation sites, the intercalation voltages and aluminum diffusion.

The crystal structures of rutile and anatase are displayed in Fig. 1. Rutile is the most common form of TiO_2 in nature, adopting the $P4_2/mnm$ space group. The TiO_6 octahedra in rutile share edges in the *c* direction and corners in the *ab* planes. While anatase belongs to the $I4_1/amd$ space group, and in the structure oxygen atoms (red balls) form edge-sharing distorted octahedra, of which half are occupied by Ti atoms, and the other half are vacant providing potential intercalation sites. The space between occupied octahedra, used for Al intercalation, is larger in anatase than that in rutile [18].

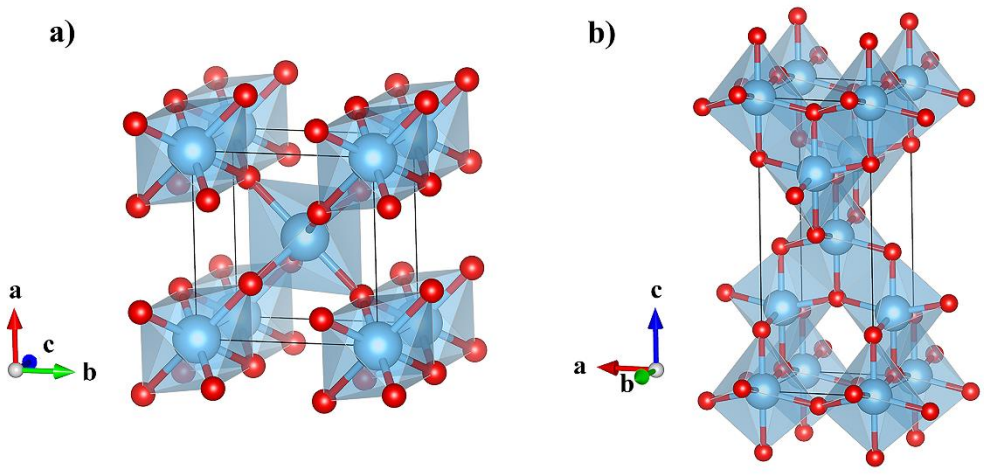

Fig. 1. A polyhedral representation of the crystal structures of a) rutile and b) anatase. Silver and red balls represent Ti and O atoms, respectively.

While the intercalation sites for lithium in different TiO_2 materials have been extensively researched [18,35-38], the stable intercalation site for aluminum is unknown in prior. Therefore, we start with the tentative intercalation site at the octahedron center, as shown in Fig. 2a and Fig. 2b, and a diffusion path analysis was thereafter performed to optimize all possible aluminum intercalation sites in rutile and anatase. Our calculation results show that the intercalation site of aluminum-ion locates in the center of the octahedral for rutile and off center position for anatase, as can be seen in Fig. 3a and Fig. 3b. For rutile, the aluminum ion remains essentially octahedral coordinated with two neighboring oxygens at 1.66 Å and four at 2.23 Å in the central site, which is consistent with previously reported results for lithium, sodium and magnesium ions [19]. For anatase, the aluminum-ion sits almost at the center of the octahedral site displaced ~ 0.05c (~ 0.5 Å) along the c direction. Similar displacement has also been reported for magnesium ions [19]. Moreover, it has been widely found that lithium (displaced 0.15 ~ 0.3 Å) and sodium ions (displaced 0.4 ~ 0.6 Å) do not sit perfectly at the center of O_6 octahedral [18,19,35,39,40].

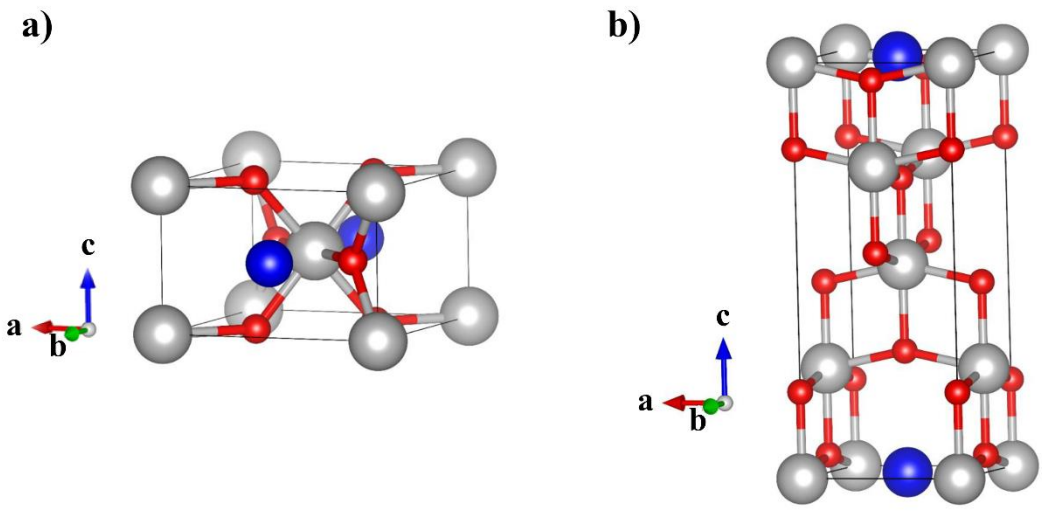

Fig. 2. Tentative intercalation sites for aluminum in a) rutile and b) anatase. Silver, red and blue balls represent Ti, O, Al (initial) atoms, respectively.

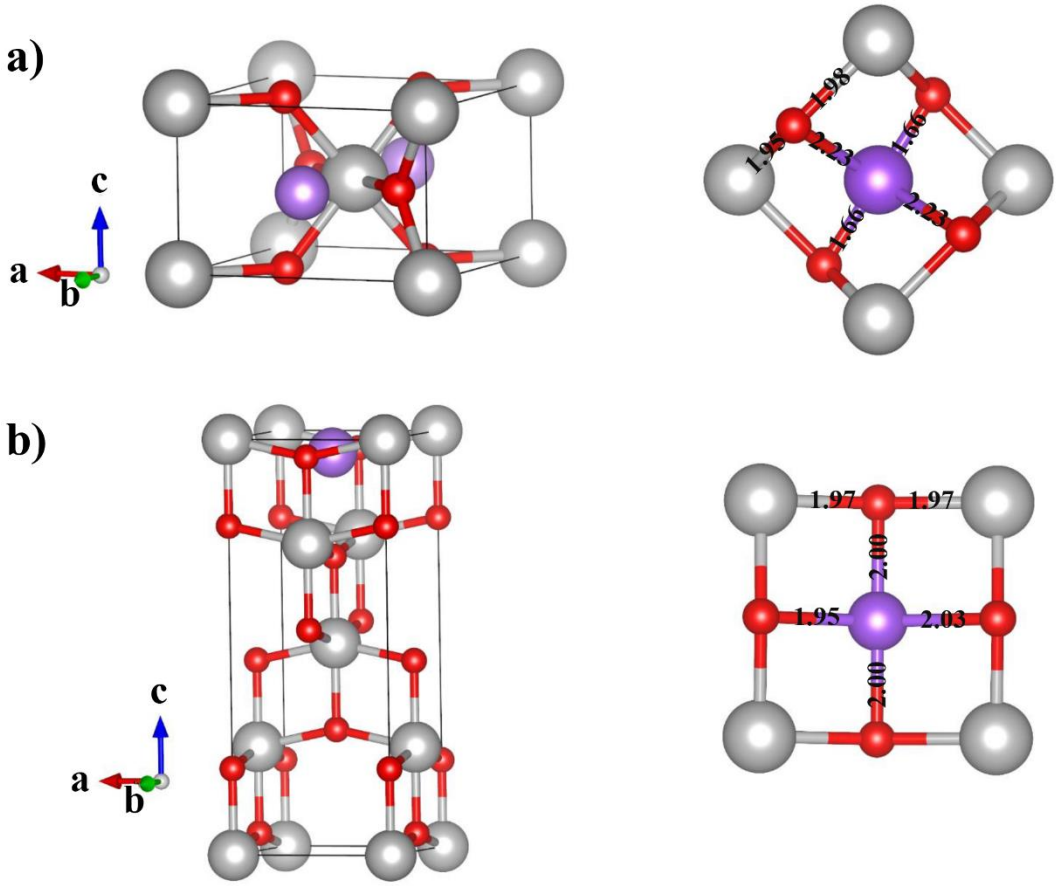

Fig. 3. Calculated intercalation sites for aluminum and schematic of the interatomic distances in c) rutile and d) anatase. Silver, red and purple balls represent Ti, O, and Al (stable) atoms, respectively. All distances are in Å.

3.2. Intercalation voltage

From the intercalation site of aluminum ions, it is found that the stability of the intercalation site of aluminum ions in the system depends mainly on two factors, i.e., the repulsive interactions between Al-Ti and between Al-Al. In $AlTi_{32}O_{64}$ for rutile or in $AlTi_{36}O_{72}$ for anatase, aluminum presents a low molar concentration (x = 0.03125 for rutile, 0.02778 for anatase), the major factor affecting the stability of aluminum implantation site arises from the repulsive force between Al-Ti. With the increase of aluminum ion concentration, the repulsion between Al-Al will increase. Therefore, it is expected that the intercalation voltage will depend on the aluminum molar ratio.

The computed average intercalation voltages profile of rutile varying with the molar ratio x in Al_xTiO_2 is shown in Fig. 4a. Not surprisingly, the average intercalation voltage decreases as the molar ratio x increases. A critical value of x is found to be 0.34375, at which the intercalation voltage drops to zero, suggesting that the intercalation of an additional aluminum atom will turn thermodynamically unfavorable when its molar ratio is greater than the critical value. The calculated average intercalation voltages profile of anatase is shown in Fig. 4a, which ranges from 0.06 to 0.77 V. As can be seen in Fig. 4b, the critical molar ratio for anatase is 0.36111 and average intercalation voltage ranges from 0.03 to 0.79 V, which are slightly higher than rutile.

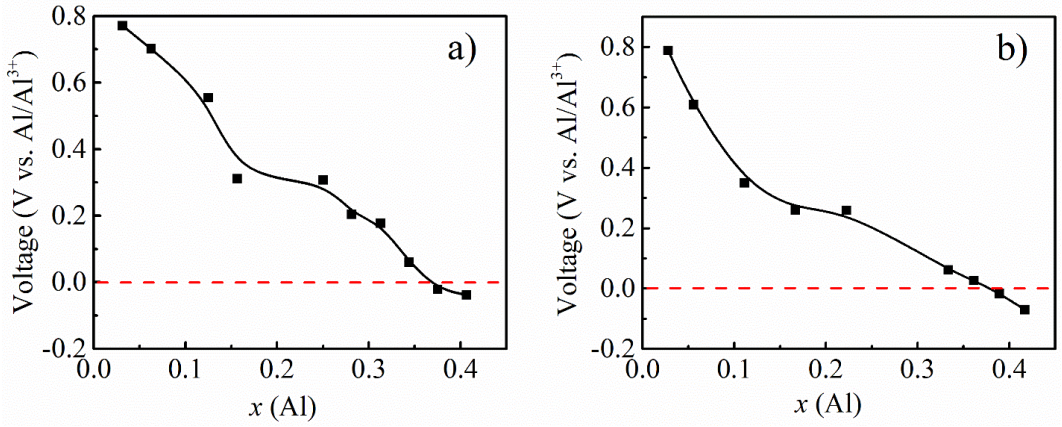

Fig. 4. Intercalation voltage for aluminum ion into Al_xTiO_2 varying with molar ratio x in different structures: a) rutile and b) anatase.

The calculated electrode capacities and energy densities for TiO_2 rutile and anatase are summarized in Table 2. The theoretical specific capacities of rutile and anatase for electrochemical aluminum storage are respectively 346.10 mAh g^{-1} and 363.58 mAh g^{-1}, which are higher than those for lithium storage. For electrochemical lithium storage, anatase [27,41] has a theoretical capacity of 335 mAh g^{-1} and rutile [42,43] has a theoretical capacity of 168 mAh g^{-1}. In addition, interestingly, the energy density of rutile is also nearly twice as high as anatase. It should be noted that higher specific energy does not necessarily give rise to higher

capacity in weight since the aluminum intercalation voltages are different for TiO_2 rutile and anatase. We note that the first principles calculation should provide more accurate estimation on energy density than the conventional thermodynamic approach upon standard thermodynamic data [44-46]. With the latter method, the energy densities for rutile and anatase are very similar [47].

Table 2. Comparison of theoretical capacities and energy densities of TiO_2 rutile and anatase.

	ΔG (kJ mol^{-1})	Gravimetric capacity (mAh g^{-1})	Volumetric capacity (mAh cm^{-3})	Specific density (Wh kg^{-1})	Energy density (Wh L^{-1})
Rutile	-6.01	346.10	1470.93	20.90	88.83
Anatase	-2.83	363.58	1414.33	9.84	38.28

3.3. Aluminiation kinetics and aluminum diffusion

The diffusion of intercalated aluminum ions is important since it determines the rate capability of an electrode. In order to examine the mobility of Al^{3+} ion, adiabatic energy surfaces for Al^{3+} ion diffusion have been computed for $x = 1/32$ (Al/Ti) in 2×2×4 rutile supercell and $x = 1/36$ (Al/Ti) in 3×3×1 anatase supercell. We examined the mobility by placing Al atoms in the adjacent octahedral positions. At each position, the energy was evaluated with fixed lattice and after full relaxation of the internal and cell coordinates.

Due to the particularity of the crystal structure and the intercalation site of rutile and anatase, in both cases only one individual diffusion pathway is found. For rutile, we examined the aluminum pathway along the [001] direction between the adjacent octahedral sites is shown in Fig. 5a, and the energy profile is shown in Fig. 5b. One possible stable interstitial site, labeled as 4, was identified between the interstitial sites X and X' in the pathway analysis. We thereafter examined the Al positions for the CI-NEB calculations, which showed that the interstitial sites of 4 and X' are very close (the distance is only 0.1 Å). In addition, by taking

optimization, we found the interstitial site 4 presents the identical energy value as X'. This indicates that the interstitial sites 4 and X' are the same position.

We continue to search the aluminum diffusion pathway between the interstitial sites X and 2 and between 2 and 4, and the energy profiles are shown in Fig. 5c and Fig. 5d. It shows that the barrier for Al diffusion is 0.34 eV. According to the transition-state theory [48] and nudged elastic band (NEB) calculations [20], the diffusivity can be calculated as [49]

$$D = (1-x)\, gvd^2 \exp\left(\frac{\Delta E_a}{k_B \mathrm{T}}\right). \quad (7)$$

In above equation, ΔE_a (kJ mol^{-1}) is the reduced activation energy required during the diffusion process with k_B (=1.38×10^{-23} J K^{-1}) being Boltzmann constant and T the system temperature (T=300 K). *g* is a geometric factor that is the reciprocal of the number of possible jump directions (*g* =1), *v* is the atomic vibration frequency in the solid crystal with typical values of 10^{12}-10^{13} s^{-1}, and *d* (Å) is the hopping distance of ions in the lattice [50]. By taking the atomic vibration frequency as 10^{13} s^{-1}, the diffusion coefficient of Al^{3+} ion in rutile is thereafter calculated to be D=10^{-9} cm^2 s^{-1}.

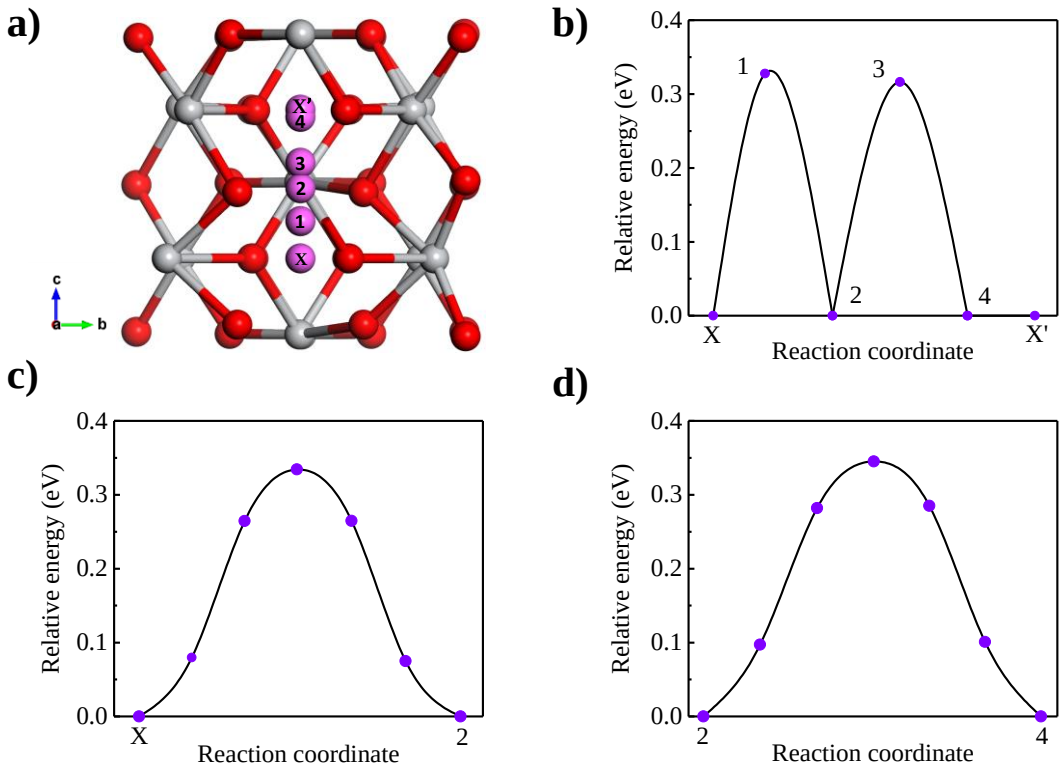

Fig. 5. a) Aluminum positions at the CI-NEB images for the GGA calculation in rutile. b) Energy profile for aluminum diffusion between adjacent octahedral in rutile, interstitial sites (X and X') are equivalent. Calculated energy profile for aluminum diffusion between c) X and 2, d) 2 and 4 of rutile. Silver, red and purple ball represent Ti, O and Al atoms, respectively.

For anatase, the calculated diffusion profile is shown in Fig. 6, and all the aluminum interstitial sites are equivalent and labeled X and X'. The calculated diffusion barrier is 1.03 eV. The diffusion coefficient is calculated to be D=10^{-20} cm^2 s^{-1}, indicating a poor mobility of aluminum ions in anatase. Examining the Al positions for the CI-NEB calculations reveals that Al^{3+} ion moving in a straight line between adjacent interstitial sites. By comparing the diffusion coefficient of Al^{3+} ion in TiO_2 rutile and anatase, we find that the mobility of Al^{3+} ions in rutile is much higher than that in anatase, indicating TiO_2 rutile offers better rate capability. It is also noted that Al^{3+} ions have lower mobility than Li^+ ions in both TiO_2 rutile and anatase. For Li^+ ions, the diffusivity ranges from 10^{-17} to 10^{-13} cm^2 s^{-1} in anatase [51-55], and is on the order of 10^{-6} cm^2 s^{-1} in rutile [38,56,57]. As our results indicate that there is only one diffusion pathway

in both the cases of anatase and rutile, the mobility of Al^{3+} ions is possibly improved by approaches such as designing oxygen deficient TiO_2 materials which may decrease the diffusion barrier and can be a subject of future studies.

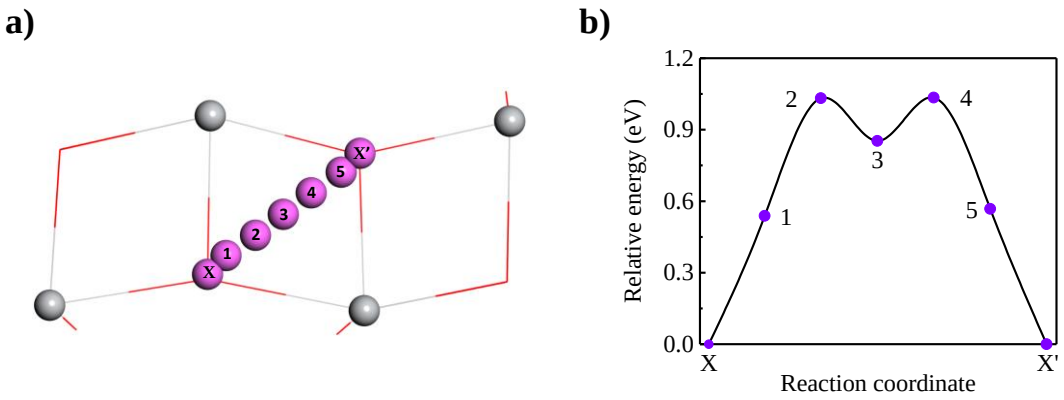

Fig. 6. a) Aluminum positions at the CI-NEB images for the GGA calculation in anatase TiO_2. b) Energy profile for aluminum diffusion between adjacent octahedral in anatase TiO_2, Interstitial sites (X and X') are equivalent. Silver and purple ball represent Ti and Al atoms, respectively.

4. Conclusions

In this study, we investigated the thermodynamic and kinetic properties of aluminum-intercalated TiO_2 rutile and anatase based on the first-principles calculation. By assessing the crystal structure, stable intercalation sites, intercalation voltage, and diffusion paths in these two common TiO_2 polymorphs, we show that the most favorable aluminum intercalation site is the center of the octahedral for rutile and off center site for anatase in Al_xTiO_2 (x<0.34375 for TiO_2 rutile, and x<0.36111 for TiO_2 anatase). The calculated intercalation voltage ranges from 0.06 to 0.77 V for rutile and from 0.03 to 0.79 V for anatase. Although rutile offers a slightly smaller theoretical capacity than anatase, its specific energy (20.90 Wh kg^{-1}) is nearly twice as high as that of anatase (9.84 Wh kg^{-1}). The diffusivities of intercalated aluminum ions in both the polymorphs are calculated, showing a low energy (~ 0.34 eV) pathway for Al^{3+}

ions diffusion along the *c*-axis channel in the [001] direction in rutile while a migration energy (~1.03 eV) along a straight line (*ac* plane) in anatase TiO_2. In addition, the diffusion coefficient of Al^{3+} ion in rutile is 10^{-9} cm^2 s^{-1}, significantly higher than that in anatase (10^{-20} cm^2 s^{-1}). From our calculations, the Al^{3+} ions present overall lower mobility than Li^+ ions in both TiO_2 rutile and anatase, whereas their theoretical capacities in rutile and anatase are higher than those for lithium storage.

In short, while both TiO_2 rutile and anatase materials present an adequate aluminum capacity for use as an electrode in rechargeable aluminum-ion batteries, TiO_2 rutile appears overall to be a better candidate than anatase as anelectrode material, which is opposite to the case for lithium ion batteries. However, the aluminum diffusion in rutile needs to be significantly enhanced to ensure attractive power performance. As our calculations indicate that there is only one diffusion pathway for rutile, designing oxygen deficient TiO_2 materials can be a potential way to reduce the diffusion barrier and thus enhance aluminum transport in the rutile materials, which can a subject of further studies.

Acknowledgements

This work is supported by National Natural Science Foundation of China (No. 91434110, U1707602), National Natural Science Foundation of China for Innovative Research Groups (No. 51621002), and the 111 Project of China (No.B08021). S. Z. acknowledges the support of Fok Ying Tong Education Foundation (151069) and W.T. is grateful to the China Scholarship Council for the visiting fellowship.

References

[1] J. Cho, S. Jeong, Y. Kim, Progress in Energy and Combustion Science, 48 (2015) 84-101.

[2] Y. Nishi, The Chemical Record, 1 (2001) 406-413.

[3] B. Dunn, H. Kamath, J.-M. Tarascon, Science, 334 (2011) 928-935.

[4] V. Etacheri, R. Marom, R. Elazari, G. Salitra, D. Aurbach, Energy and Environmental Science, 4 (2011) 3243-3262.

[5] M.P. Paranthaman, G. Brown, X.-G. Sun, J. Nanda, A. Manthiram, A. Manivannan, in: Meeting Abstracts, The Electrochemical Society, 2010, pp. 314.

[6] S.K. Das, S. Mahapatra, H. Lahan, Journal of Materials Chemistry A, 5 (2017) 6347-6367.

[7] Z.A. Zafar, S. Imtiaz, R. Razaq, S. Ji, T. Huang, Z. Zhang, Y. Huang, J.A. Anderson, Journal of Materials Chemistry A, 5 (2017) 5646-5660.

[8] T. Koketsu, J. Ma, B.J. Morgan, M. Body, C. Legein, W. Dachraoui, M. Giannini, A. Demortière, M. Salanne, F. Dardoize, Nature Materials, 16 (2017) 1142-1148.

[9] L. Kavan, M. Grätzel, S. Gilbert, C. Klemenz, H. Scheel, Journal of the American Chemical Society, 118 (1996) 6716-6723.

[10] S. Liu, J. Hu, N. Yan, G. Pan, G. Li, X. Gao, Energy and Environmental Science, 5 (2012) 9743-9746.

[11] Y.J. He, J.F. Peng, W. Chu, Y.Z. Li, D.G. Tong, Journal of Materials Chemistry A, 2 (2014) 1721-1731.

[12] M. Kazazi, P. Abdollahi, M. Mirzaei-Moghadam, Solid State Ionics, 300 (2017) 32-37.

[13] M. Ojeda, B. Chen, D.Y. Leung, J. Xuan, H. Wang, Energy Procedia, 105 (2017) 3997-4002.

[14] G. Kresse, J. Hafner, Physical Review B, 47 (1993) 558-561.

[15] G. Kresse, J. Furthmüller, Physical Review B Condensed Matter, 54 (1996) 11169-11196.

[16] P.E. Blöchl, Physical Review B, 50 (1994) 17953-17979.

[17] G. Kresse, D. Joubert, Physical Review B Condensed Matter, 59 (1999) 1758-1775.

[18] J.A. Dawson, J. Robertson, Journal of Physical Chemistry C, 120 (2016) 22910-22917.

[19] F. Legrain, O. Malyi, S. Manzhos, Journal of Power Sources, 278 (2015) 197-202.

[20] G. Henkelman, B.P. Uberuaga, H. Jónsson, Journal of Chemical Physics, 113 (2000) 9901-9904.

[21] M.K. Aydinol, A.F. Kohan, G. Ceder, K. Cho, J. Joannopoulos, Physical Review B Condensed Matter, 56 (1997) 1353-1365.

[22] L.I. Bendavid, E.A. Carter, The Journal of Physical Chemistry C, 117 (2013) 26048-26059.

[23] J.S. Braithwaite, C.R.A. Catlow, J.H. Harding, J.D. Gale, Physical Chemistry Chemical Physics, 3 (2001) 4052-4059.

[24] I.B. Rumpf, Veterinary Immunology and Immunopathology, 55 (1997) 359-360.

[25] S. Begin-Colin, G.L. Caer, A. Mocellin, M. Zandona, Philosophical magazine letters, 69 (1994) 1-7.

[26] P. Bose, S. Pradhan, S. Sen, Materials chemistry and physics, 80 (2003) 73-81.

[27] S.K. Das, S. Darmakolla, A.J. Bhattacharyya, Journal of Materials Chemistry, 20 (2010) 1600-1606.

[28] G. Ceder, Y.M. Chiang, D.R. Sadoway, M.K. Aydinol, Y.I. Jang, B. Huang, Nature, 392 (1998) 694-696.

[29] V.I. Anisimov, J. Zaanen, O.K. Andersen, Physical Review B Condensed Matter, 44 (1991) 943.

[30] B.J. Morgan, G.W. Watson, Surface Science, 601 (2007) 5034-5041.

[31] M. Nolan, S.D. Elliott, J.S. Mulley, R.A. Bennett, M. Basham, P. Mulheran, Physical Review B, 77 (2008) 235424.

[32] S.L. Dudarev, G.A. Botton, S.Y. Savrasov, C.J. Humphreys, A.P. Sutton, Physical Review B, 57 (1998) 1505-1509.

[33] S.C. Abrahams, J.L. Bernstein, Journal of Chemical Physics, 55 (1971) 3206-3211.

[34] M. Horn, C.F. Schwerdtfeger, E.P. Meagher, Zeitschrift Für Kristallographie, 136 (1972) 273-281.

[35] B.J. Morgan, G.W. Watson, Physical Review B, 82 (2010) 144119.

[36] C. Arrouvel, S.C. Parker, M.S. Islam, Chemistry of Materials, 21 (2009) 4778-4783.

[37] A. Stashans, S. Lunell, R. Bergström, A. Hagfeldt, S.-E. Lindquist, Physical Review B, 53 (1996) 159.

[38] M.V. Koudriachova, N.M. Harrison, S.W. de Leeuw, Physical Review B, 65 (2002) 235423.

[39] M. Wagemaker, G.J. Kearley, A.A. Van Well, H. Mutka, F.M. Mulder, Journal of the American Chemical Society, 125 (2003) 840-848.

[40] H. Sun, Journal of Physical Chemistry B, 102 (1998) 7338-7364.

[41] K. Liang, X. Chen, Z. Guo, T. Hou, X. Zhang, Y. Li, Physical Chemistry Chemical Physics, 18 (2016) 24370-24376.

[42] K.-S. Park, K.-M. Min, Y.-H. Jin, S.-D. Seo, G.-H. Lee, H.-W. Shim, D.-W. Kim, Journal of Materials Chemistry, 22 (2012) 15981-15986.

[43] T. Zeng, P. Ji, X. Hu, G. Li, RSC Advances, 6 (2016) 48530-48536.

[44] I. Barin, Thermodymamical Data of Pure Substances, 3rd Edition, VCH, Weinheim, Germany, 1995.

[45] R. David, CRC Handbook of Chemistry and Physics, 90th Edition, CRC Press, Boca Raton FL, 2009.

[46] J.G. Speight, Lange's Handbook of Chemistry, 16th Edition, McGrawHill, New York, 2005.

[47] C.-X. Zu, H. Li, Energy and Environmental Science, 4 (2011) 2614-2624.

[48] G.H. Vineyard, Journal of Physics and Chemistry of Solids, 3 (1957) 121-127.

[49] R. Kutner, Physics Letters A, 81 (1981) 239-240.

[50] G. Yoon, D.H. Kim, I. Park, D. Chang, B. Kim, B. Lee, K. Oh, K. Kang, Advanced Functional Materials, 27 (2017).

[51] K. Kanamura, K. Yuasa, Z. Takehara, Journal of Power Sources, 20 (1987) 127-134.

[52] L. Kavan, J. Rathouský, M. Grätzel, V. Shklover, A. Zukal, The Journal of Physical Chemistry B, 104 (2000) 12012-12020.

[53] M.P. Cantao, J.I. Cisneros, R.M. Torresi, The Journal of Physical Chemistry, 98 (1994) 4865-4869.

[54] H. Lindström, S. Södergren, A. Solbrand, H. Rensmo, J. Hjelm, A. Hagfeldt, S.-E. Lindquist, The Journal of Physical Chemistry B, 101 (1997) 7710-7716.

[55] R. van de Krol, A. Goossens, J. Schoonman, The Journal of Physical Chemistry B, 103 (1999) 7151-7159.

[56] O.W. Johnson, Physical Review, 136 (1964) A284.

[57] F. Gligor, S.W. de Leeuw, Solid State Ionics, 177 (2006) 2741-2746.